SCIENCE CHINA
Information Sciences

August 2019, Vol. 62 080301:1–080301:17
https://doi.org/10.1007/s11432-018-9808-5

• RESEARCH PAPER •
Special Focus on B5G Wireless Communication Networks

Fast-convolution multicarrier based frequency division multiple access

Yining LI, Wenjin WANG, Jiaheng WANG & Xiqi GAO*

National Mobile Communications Research Laboratory, Southeast University, Nanjing 210096, *China*

Received 5 December 2018/Revised 26 February 2019/Accepted 1 March 2019/Published online 11 July 2019

Abstract Fast-convolution multicarrier (FCMC), the asynchronous waveform with ultra-low sidelobe, has appeared to be a promising waveform technique for future wireless communications. In this paper, we investigate the filter bank optimization as well as receiver design including low-complexity channel estimator and equalizer for FCMC based frequency division multiple access (FDMA). Starting from the conventional multi-carrier signals, we first derive a vectorized signal model as a framework to systematically design the FCMC transceiver. For nearly perfect reconstruction (NPR) filter banks design, an optimization criterion which consists of minimizing received signal segments' mean square error (MSE) is proposed. From the fact that Toeplitz matrices can be asymptotically diagonalized by discrete Fourier transform (DFT) matrix, the channel equalizer can be simplified to one-tap frequency domain equalizer when DFT size is large enough. The minimum mean square error (MMSE) criterion is then applied to calculate the coefficients of one-tap frequency domain equalizer. In practice, due to the channel fading, the channel estimation has to be performed to obtain the channel state information (CSI) which is required by the channel equalization. To this end, we propose a combined cyclic prefix (CP) and cyclic suffix (CS) pilot structure which facilitates to estimate the frequency domain CSI directly in the receiver end. The proposed FCMC based FDMA features low-complexity receiver, adjustable users' bandwidth and low peak-to-average power ratio. Simulation results confirm the performance of the proposed scheme.

Keywords multirate signal processing, filter banks, fast convolution, channel estimation, equalizer

Citation Li Y N, Wang W J, Wang J H, et al. Fast-convolution multicarrier based frequency division multiple access. Sci China Inf Sci, 2019, 62(8): 080301, https://doi.org/10.1007/s11432-018-9808-5

1 Introduction

In the past decades, orthogonal frequency division multiplexing (OFDM) has enjoyed its dominance as the most popular signaling method for broadband communications. The fifth-generation (5G) and beyond 5G (B5G) wireless communication networks are required to support the scenarios of different types including higher data rates, lower transmission delays, and massive connectivities. However, it has been noted that OFDM faces many challenges when considered for 5G/B5G wireless networks [1, 2]. For instance, its poor frequency localization, strong out-of-band emission (OOBE) and suboptimal spectrum shape make it inadequate to asynchronous applications [3–5]. Currently, many researchers are exploring alternative waveforms to avoid such limitations of OFDM. For example, filter bank multicarrier (FBMC) [6–8], generalized frequency division multiplexing (GFDM) [9], filtered-OFDM (F-OFDM) [10], universal filtered multicarrier (UFMC) [11] and fast convolution multicarrier (FCMC) are raised as waveform candidates due to their superiorities over OFDM [12], i.e., achievements in subbands asynchronization and lower

* Corresponding author (email: xqgao@seu.edu.cn)

OOBE. Therefore, designing a waveform which of lower complexity and better spectral performance than OFDM is significant in 5G/B5G wireless systems.

Compared with FBMC and GFDM, filter banks in FCMC systems are implemented with low complexity [13]. Therefore, it is promising to investigate the filter banks and low-complexity receiver design in FCMC system. The main idea of fast convolution (FC) is that a high-order filter can be implemented effectively through multiplication in the frequency domain, after taking discrete Fourier transform (DFT) of the input sequences and the filter impulse response. FC implementation is confirmed to provide high flexibility and convenience in frequency domain filtering. The application of FC to multirate filters has been presented in [14, 15]. Furthermore, the FC implementation of nearly perfect reconstruction (NPR) filter banks systems has been developed in [16]. Due to the achievements of low complexity filter implementation, FC approach has been applied to filter bank multicarrier [17], filtered-OFDM [18, 19], and single-carrier waveforms [20].

Different from prototype filter impulse response coefficients design in FBMC systems [21–23], fast convolution filter banks (FC-FB) design was stated as the problem to find the optimal values of the frequency domain window for multiple subbands. Since filter banks with different center frequencies can be obtained by a single low-pass subband filter shifting in the frequency domain, the optimization problem of frequency domain filter banks design is simplified to the optimization of the prototype frequency domain window. The root-raised-cosine (RRC)/raised-cosine (RC) filters were applied as the prototype filter bank, and the characteristics of them were demonstrated in [16]. However, the prototype filter bank optimization problems have not been solved in the recent literature.

In particular, the multipath fading that commonly exists in a wireless communication environment leads to severe inter symbol interference (ISI). In order to achieve reliable communication, channel equalization is necessary to combat ISI. The embedded one-tap equalization structure which fits the FC filter banks was put forward in [24]. The equalizer contains pulse-shaping matched filter, channel matched filter, decimator and linear equalizer with minimum mean square error (MMSE) criterion. It was demonstrated that the embedded equalization model reduces arithmetic complexity in comparison to multi-tap subcarrier equalizers. An FC-version one-tap MMSE frequency domain equalizer without CP was derived in [25]. However, low-complexity channel equalizer combining filter banks equalization and physical channel equalization applied in FCMC system have not been developed in the recent literature. In addition, how to obtain the channel state information (CSI) that is required by the channel equalization is not straightforward. This will be another issue that we investigate here.

In this study, we propose a straightforward method to optimize synthesis and analysis filter banks such that the inter band interference (IBI) and OOBE can be minimized with respect to energy and subcarriers range constraints. We derive the ideal one-tap MMSE equalizer in order to minimize the mean square error (MSE) of the recovered baseband signal, but this one-tap equalizer coefficients calculation is of high complexity. Furthermore, we develop the low-complexity one-tap MMSE frequency domain equalizer exploiting asymptotic behavior of Toeplitz matrices. In order to acquire the frequency domain CSI required by the equalizer, we choose to insert time domain pilot which makes no damage to the modulated signal power spectrum. A pilot structure called combined cyclic prefix (CP) and cyclic suffix (CS) structure is presented in order to simplify CSI estimation.

The rest of this paper is organized as follows. The FCMC system model including the ideal and multipath channel is built in Section 2. Then in Section 3, received signal error is quantified, and the reconstruction error is minimized to design filter banks. In Section 4, we propose the MMSE frequency domain equalizer (FDE) which combines analysis filter banks and the physical channel equalizer together. From the fact that Toeplitz matrices can be asymptotically diagonalized by DFT matrix, the one-tap equalizer can be simplified without system performance degradation. In Section 5, the time domain pilot structure is exploited, and subband estimator is derived based on the designed pilot. Simulation results are presented in Section 6. Conclusion is drawn in Section 7.

Notations. We use upper (lower) bold-face letters to denote matrices (column vectors). An $N \times N$ identity matrix is denoted by $\boldsymbol{I}_N$, an all-zero matrix is denoted by $\mathbf{0}$, and an $M \times N$ all-one matrix is denoted by $\mathbf{1}_{M\times N}$. The kth column vector of an identity matrix is denoted by $\boldsymbol{e}_k$ with the dimension

being determined from the context. Superscripts H, T, and * denote Hermitian transpose, transpose, and conjugate, respectively. We reserve $\otimes$ for Kronecker product, E{} for expectation, $((n))_M$ for n modulo M. $[\boldsymbol{a}]_m$ denotes the mth element of vector $\boldsymbol{a}$. The vec-operator denoted as vec($\boldsymbol{X}$) stacks the columns of $\boldsymbol{X}$ into a vector. $\|\cdot\|_F$ and $\|\cdot\|_2$ denote normalized Frobenius norm and 2-norm operator separately. We use diag($\boldsymbol{x}$) for a diagonal matrix with its diagonal elements being $\boldsymbol{x}$, circ($\boldsymbol{x}$) for a circulant matrix with first column $\boldsymbol{x}$.

2 System model

2.1 Fast convolution multicarrier

Assume $x_u(n)$ is the baseband oversampled time domain signal of the uth subband and given by

$$x_u(n) = \sum_{m=-\infty}^{\infty} s_u(m) g_u(n - mN_{r,u}), \tag{1}$$

where $s_u(m)$ represents the mth symbol of modulated signal stream for the uth subband with low sampling rate, $g_u(n)$ represents the symmetric and non-causal lowpass filter for pulse shaping, $N_{r,u}$ represents the oversampling factor for the uth subband. Suppose $g_u(n)$ takes non-zero values for $-L \leqslant n \leqslant L-1$. It should be noted that the sampling rate of $g_u(n)$ and $x_u(n)$ is $N_{r,u}$ times that of $s_u(m)$.

Let

$$s'_u(n) = \begin{cases} s_u(m), & n = mN_{r,u}, \\ 0, & \text{otherwise.} \end{cases} \tag{2}$$

Thus, Eq. (1) can be rewritten as

$$x_u(n) = \sum_{m=-\infty}^{\infty} s'_u(m) g_u(n - m). \tag{3}$$

Filtering for a long signal is usually operated with dividing it into multiple segments. In each segment, FFT may be used to realize fast convolution in the frequency domain. Overlap-save and overlap-add method are two basic methods used for convolving long data records [26]. The overlap-save method is commonly applied in FCMC system for the reason that the latter one may induce noise when adding two sequences together.

In overlap-save based FCMC, data is divided into blocks of length M with successive blocks overlapping by L. The kth overlapped sample block $s'_u(n)$ and $g_{u,o}(n)$ are defined as follows:

$$\begin{aligned} s'_{u,k}(n) &= s'_u(n + kN - L + 1),\ n = 0, 1, \ldots, M-1, \\ g_{u,o}(n) &= \begin{cases} g_u(n), & 0 \leqslant n \leqslant L-1, \\ 0, & L \leqslant n \leqslant N + L - 1, \\ g_u(n - M), & N + L \leqslant n \leqslant M - 1, \end{cases} \end{aligned} \tag{4}$$

where $N = M - 2L$. Therefore, the kth output block record is

$$x_{u,k}(n - L) = \sum_{m=0}^{M-1} g_{u,o}(m) s'_{u,k}((n-m))_M,\ n = L, L+1, \ldots, L+N-1. \tag{5}$$

The linear convolution output of $s'_u(n)$ and $g_u(n)$ is formed by concatenating all such records, thus we have

$$x_u(n + kN) = x_{u,k}(n), \quad k = 0, 1, \ldots. \tag{6}$$

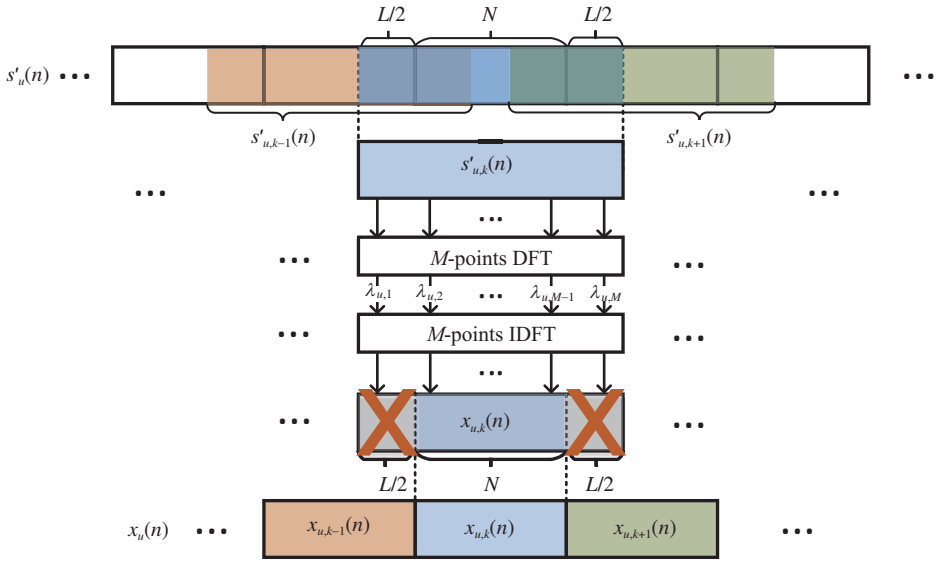

Figure 1 (Color online) Overlap-save processing on the transmitter side.

Let $\boldsymbol{s}'_{u,k} = [s'_{u,k}(0) \ \cdots \ s'_{u,k}(M-1)]^{\mathrm{T}}$, $\boldsymbol{x}_{u,k} = [x_{u,k}(0) \ \cdots \ x_{u,k}(N-1)]^{\mathrm{T}}$ denote the kth overlapped interpolated data segment and transmitted data segment of the uth subband, respectively. $\boldsymbol{g}_{u,o} = [g_{u,o}(0) \ \cdots \ g_{u,o}(M-1)]^{\mathrm{T}}$. The matrix form of (5) can be written as

$$\boldsymbol{x}_{u,k} = \boldsymbol{Q}\mathrm{circ}(\boldsymbol{g}_{u,o})\boldsymbol{s}'_{u,k}, \tag{7}$$

where $\boldsymbol{Q} = [\,\boldsymbol{0}_{N\times L} \ \boldsymbol{I}_N \ \boldsymbol{0}_{N\times L}\,]$. Circulant matrix $\mathrm{circ}(\boldsymbol{g}_{u,o})$ can be diagonalized by DFT and IDFT matrices, so that Eq. (7) is further simplified to

$$\boldsymbol{x}_{u,k} = \boldsymbol{Q}\boldsymbol{W}_M^{\mathrm{H}}\boldsymbol{\Lambda}_u\boldsymbol{W}_M\boldsymbol{s}'_{u,k}, \tag{8}$$

where $\boldsymbol{W}_M^{\mathrm{H}}$ and $\boldsymbol{W}_M$ are normalized M-points IDFT and DFT matrices, $\boldsymbol{\Lambda}_u = \mathrm{diag}(\boldsymbol{\lambda}_u)$, $\boldsymbol{\lambda}_u = \boldsymbol{W}_M\boldsymbol{g}_{u,o}$. The overlapping-save processing of (8) is shown in Figure 1.

Let $M_{b,u} = M/N_{r,u}$, $N_{b,u} = N/N_{r,u}$, $L_{b,u} = L/N_{r,u}$, $s_{u,k}(n) = s_u(n+kN_{b,u}+1), n = 0,1,\ldots,N_{b,u}-1$, and $\boldsymbol{s}_{u,k} = [s_{u,k}(0) \ \cdots \ s_{u,k}(N_{b,u}-1)]^{\mathrm{T}}$, then $\boldsymbol{s}'_{u,k}$ can be expressed in the form as follows:

$$\boldsymbol{s}'_{u,k} = \boldsymbol{P}(\boldsymbol{I}_3 \otimes \boldsymbol{\Gamma}_{b,u})\left[\,\boldsymbol{s}_{u,k-1}^{\mathrm{T}} \ \boldsymbol{s}_{u,k}^{\mathrm{T}} \ \boldsymbol{s}_{u,k+1}^{\mathrm{T}}\,\right]^{\mathrm{T}}, \tag{9}$$

where $\boldsymbol{P} = [\,\boldsymbol{0}_{M\times(N-L)} \ \boldsymbol{I}_M \ \boldsymbol{0}_{M\times(N-L)}\,]$, $\boldsymbol{\Gamma}_{b,u} = \boldsymbol{I}_{N_{b,u}} \otimes \boldsymbol{e}_1$ is the $N_{r,u}$-fold interpolation matrix, and the dimension of $\boldsymbol{e}_1$ is $N_{r,u}$. Substituting (9) into (8), we have

$$\boldsymbol{x}_{u,k} = \boldsymbol{Q}\boldsymbol{W}_M^{\mathrm{H}}\boldsymbol{\Lambda}_u\boldsymbol{W}_M\boldsymbol{P}(\boldsymbol{I}_3 \otimes \boldsymbol{\Gamma}_{b,u})\left[\,\boldsymbol{s}_{u,k-1}^{\mathrm{T}} \ \boldsymbol{s}_{u,k}^{\mathrm{T}} \ \boldsymbol{s}_{u,k+1}^{\mathrm{T}}\,\right]^{\mathrm{T}}. \tag{10}$$

As derived in [25], the matrix-form model of FCMC transmitter can be simplified to

$$\boldsymbol{x}_{u,k} = \boldsymbol{Q}\boldsymbol{W}_M^{\mathrm{H}}\boldsymbol{\Lambda}_u\boldsymbol{E}_u\boldsymbol{W}_{M_{b,u}}\boldsymbol{P}_{b,u}\left[\,\boldsymbol{s}_{u,k-1}^{\mathrm{T}} \ \boldsymbol{s}_{u,k}^{\mathrm{T}} \ \boldsymbol{s}_{u,k+1}^{\mathrm{T}}\,\right]^{\mathrm{T}}, \tag{11}$$

where $\boldsymbol{E}_u = \boldsymbol{1}_{N_{r,u}\times 1}\otimes\boldsymbol{I}_{M_{b,u}}$, $\boldsymbol{P}_{b,u} = [\,\boldsymbol{0}_{M_{b,u}\times(N_{b,u}-L_{b,u})} \ \boldsymbol{I}_{M_{b,u}} \ \boldsymbol{0}_{M_{b,u}\times(N_{b,u}-L_{b,u})}\,]$. The simplifed transmitter implementation includes blocks overlapping, $M_{b,u}$-points FFT, frequency spread, filtering, M-points IFFT, and samples discarding. Comparing (11) with (10), we can obtain interpolated frequency domain signal more efficiently.

Let $\boldsymbol{y}_{u,k}$ and $\hat{\boldsymbol{s}}_{u,k}$ denote the kth received and demodulated data block of the uth subband. The matrix-form model of FCMC receiver is

$$\hat{\boldsymbol{s}}_{u,k} = \boldsymbol{Q}_{b,u}\boldsymbol{W}_{M_{b,u}}^{\mathrm{H}}\boldsymbol{E}_u^{\mathrm{T}}\boldsymbol{\Lambda}_u^{\mathrm{H}}\boldsymbol{W}_M\boldsymbol{P}\left[\boldsymbol{y}_{u,k-1}^{\mathrm{T}} \ \boldsymbol{y}_{u,k}^{\mathrm{T}} \ \boldsymbol{y}_{u,k+1}^{\mathrm{T}}\right]^{\mathrm{T}}, \tag{12}$$

where $\boldsymbol{Q}_{b,u} = [\,\boldsymbol{0}_{N_{b,u}\times L_{b,u}}\ \boldsymbol{I}_{N_{b,u}}\ \boldsymbol{0}_{N_{b,u}\times L_{b,u}}\,]$. Notice that $\boldsymbol{\Lambda}_u$ is a real matrix when $g_{u,o}(n)$ is a symmetric and non-causal filter.

2.2 Fast convolution multicarrier based FDMA in multipath fading channel

We consider a multiuser FCMC system based on frequency division multiple access (FDMA), where each user equipment (UE) occupies different subbands in the frequency domain. The baseband multicarrier signal in the downlink transmission can be written as

$$x^{\mathrm{DL}}(n) = \sum_{u=1}^{U} x_u(n), \tag{13}$$

where $x^{\mathrm{DL}}(n)$ denotes transmitted baseband data stream in downlink transmission. Combining (6) and (13), $x^{\mathrm{DL}}(n)$ can be rewritten as

$$x^{\mathrm{DL}}(n+kN) = \sum_{u=1}^{U} x_{u,k}(n-kN), \quad k = 0, 1, \ldots. \tag{14}$$

The following is time and frequency domain received signal model analysis under multipath fading channels. Let $\boldsymbol{H}_u$ denote the channel matrix of the uth subband. $\boldsymbol{H}_u$ is a $3N\times 3N$ nonsymmetric Toeplitz matrix with channel impulse response $[\tilde{h}_0\ \cdots\ \tilde{h}_{L_{\mathrm{ch}}}\ 0\ \cdots\ 0]^{\mathrm{T}}$ being its first column and $[\tilde{h}_0\ 0\ \cdots\ 0]$ being its first row, where $\tilde{h}_i$ is the ith tap coefficient of the multipath channel. L_{ch} is the length of the multipath channel. $\hat{\boldsymbol{y}}_{u,k}^{\mathrm{DL}}$ and $\hat{\boldsymbol{y}}_{u,k}^{\mathrm{UL}}$ are the kth overlapped received block in downlink and uplink transmission. $\hat{\boldsymbol{y}}_{u,k}^{\mathrm{DL}}$ and $\hat{\boldsymbol{y}}_{u,k}^{\mathrm{UL}}$ are written as

$$\hat{\boldsymbol{y}}_{u,k}^{\mathrm{DL}} = \boldsymbol{P}\boldsymbol{H}_u \sum_{u=1}^{U} \underline{\boldsymbol{x}}_{u,k} + \boldsymbol{z}_{u,k}, \tag{15}$$

and

$$\hat{\boldsymbol{y}}_{k}^{\mathrm{UL}} = \boldsymbol{P} \sum_{u=1}^{U} \boldsymbol{H}_u \underline{\boldsymbol{x}}_{u,k} + \boldsymbol{z}_{k}, \tag{16}$$

where $\underline{\boldsymbol{x}}_{u,k} = [\boldsymbol{x}_{u,k-1}^{\mathrm{T}}\ \boldsymbol{x}_{u,k}^{\mathrm{T}}\ \boldsymbol{x}_{u,k+1}^{\mathrm{T}}]^{\mathrm{T}}$, $\boldsymbol{z}_k$ is channel noise of Gaussian distribution with zero mean. Notice that received signal model in downlink transmission can be regarded as a special case of that in uplink transmission with $\boldsymbol{H}_{u'} = \boldsymbol{H}_u, \forall u' \neq u$. For the purpose of simplicity and generality, we ignore superscript UL and DL and consider the uplink transmission in the following.

Let $\hat{\boldsymbol{y}}_k^f = \boldsymbol{W}_M \hat{\boldsymbol{y}}_k$ denote the kth frequency domain received data block of the uth UE. Substituting (11) to (16), we have

$$\hat{\boldsymbol{y}}_k^f = \sum_{u=1}^{U} \hat{\boldsymbol{y}}_{u,k}^f, \tag{17}$$

and

$$\hat{\boldsymbol{y}}_{u,k}^f = \sum_{k'=-2}^{2} \boldsymbol{C}_{k',u}\boldsymbol{s}_{u,k+k'} + \tilde{\boldsymbol{z}}_{u,k}, \tag{18}$$

where $\boldsymbol{C}_{k',u}$ is given by

$$\begin{aligned}
\boldsymbol{C}_{-2,u} &= \boldsymbol{W}_M\boldsymbol{H}_{P,u,-1}\boldsymbol{Q}\boldsymbol{W}_M^{\mathrm{H}}\boldsymbol{\Lambda}_u\boldsymbol{E}_u\boldsymbol{W}_{M_{b,u}}\boldsymbol{P}_{b,u,-1},\\
\boldsymbol{C}_{-1,u} &= \boldsymbol{W}_M\boldsymbol{H}_{P,u,-1}\boldsymbol{Q}\boldsymbol{W}_M^{\mathrm{H}}\boldsymbol{\Lambda}_u\boldsymbol{E}_u\boldsymbol{W}_{M_{b,u}}\boldsymbol{P}_{b,u,0} + \boldsymbol{W}_M\boldsymbol{H}_{P,u,0}\boldsymbol{Q}\boldsymbol{W}_M^{\mathrm{H}}\boldsymbol{\Lambda}_u\boldsymbol{E}_u\boldsymbol{W}_{M_{b,u}}\boldsymbol{P}_{b,u,-1},\\
\boldsymbol{C}_{0,u} &= \boldsymbol{W}_M\boldsymbol{H}_{P,u,-1}\boldsymbol{Q}\boldsymbol{W}_M^{\mathrm{H}}\boldsymbol{\Lambda}_u\boldsymbol{E}_u\boldsymbol{W}_{M_{b,u}}\boldsymbol{P}_{b,u,1} + \boldsymbol{W}_M\boldsymbol{H}_{P,u,0}\boldsymbol{Q}\boldsymbol{W}_M^{\mathrm{H}}\boldsymbol{\Lambda}_u\boldsymbol{E}_u\boldsymbol{W}_{M_{b,u}}\boldsymbol{P}_{b,u,0}\\
&\quad + \boldsymbol{W}_M\boldsymbol{H}_{P,u,1}\boldsymbol{Q}\boldsymbol{W}_M^{\mathrm{H}}\boldsymbol{\Lambda}_u\boldsymbol{E}_u\boldsymbol{W}_{M_{b,u}}\boldsymbol{P}_{b,u,-1},\\
\boldsymbol{C}_{1,u} &= \boldsymbol{W}_M\boldsymbol{H}_{P,u,0}\boldsymbol{Q}\boldsymbol{W}_M^{\mathrm{H}}\boldsymbol{\Lambda}_u\boldsymbol{E}_u\boldsymbol{W}_{M_{b,u}}\boldsymbol{P}_{b,u,1} + \boldsymbol{W}_M\boldsymbol{H}_{P,u,1}\boldsymbol{Q}\boldsymbol{W}_M^{\mathrm{H}}\boldsymbol{\Lambda}_u\boldsymbol{E}_u\boldsymbol{W}_{M_{b,u}}\boldsymbol{P}_{b,u,0},\\
\boldsymbol{C}_{2,u} &= \boldsymbol{W}_M\boldsymbol{H}_{P,u,1}\boldsymbol{Q}\boldsymbol{W}_M^{\mathrm{H}}\boldsymbol{\Lambda}_u\boldsymbol{E}_u\boldsymbol{W}_{M_{b,u}}\boldsymbol{P}_{b,u,1}.
\end{aligned} \tag{19}$$

$\tilde{\boldsymbol{z}}_{u,k}$ is the summation of adjacent subbands' interferences and environmental noise. $\boldsymbol{P}_b$ is partitioned to three blocks of same size in the form $\boldsymbol{P}_{b,u} = [\boldsymbol{P}_{b,u,-1}\ \boldsymbol{P}_{b,u,0}\ \boldsymbol{P}_{b,u,1}]$. Similarly, $\boldsymbol{P}$ is partitioned into three blocks of same size in the form as $\boldsymbol{P} = [\boldsymbol{P}_{-1}\ \boldsymbol{P}_0\ \boldsymbol{P}_1]$. $\boldsymbol{H}_{P,u,i} = \boldsymbol{P}_i\boldsymbol{H}_u, i = -1, 0, 1$.

The matrix form of (18) can be written as follows:

$$\hat{\boldsymbol{y}}_{u,k} = \boldsymbol{H}_{P,u}\begin{bmatrix} \boldsymbol{H}_{\boldsymbol{\Lambda},u,-1} & \boldsymbol{H}_{\boldsymbol{\Lambda},u,0} & \boldsymbol{H}_{\boldsymbol{\Lambda},u,1} & & \\ & \boldsymbol{H}_{\boldsymbol{\Lambda},u,-1} & \boldsymbol{H}_{\boldsymbol{\Lambda},u,0} & \boldsymbol{H}_{\boldsymbol{\Lambda},u,1} & \\ & & \boldsymbol{H}_{\boldsymbol{\Lambda},u,-1} & \boldsymbol{H}_{\boldsymbol{\Lambda},u,0} & \boldsymbol{H}_{\boldsymbol{\Lambda},u,1} \end{bmatrix}(\boldsymbol{I}_5 \otimes \boldsymbol{\Gamma}_{b,u})\begin{bmatrix} \boldsymbol{s}_{u,k-2} \\ \boldsymbol{s}_{u,k-1} \\ \boldsymbol{s}_{u,k} \\ \boldsymbol{s}_{u,k+1} \\ \boldsymbol{s}_{u,k+2} \end{bmatrix} + \tilde{\boldsymbol{z}}_{u,k}, \tag{20}$$

where $\boldsymbol{H}_{\boldsymbol{\Lambda},u,i} = \boldsymbol{Q}\boldsymbol{W}_M^{\mathrm{H}}\boldsymbol{\Lambda}_u\boldsymbol{W}_M\boldsymbol{P}_i, i = -1, 0, 1$. Let

$$\boldsymbol{H}_{\mathrm{eq},u} = \boldsymbol{H}_{P,u}\begin{bmatrix} \boldsymbol{H}_{\boldsymbol{\Lambda},u,-1} & \boldsymbol{H}_{\boldsymbol{\Lambda},u,0} & \boldsymbol{H}_{\boldsymbol{\Lambda},u,1} & & \\ & \boldsymbol{H}_{\boldsymbol{\Lambda},u,-1} & \boldsymbol{H}_{\boldsymbol{\Lambda},u,0} & \boldsymbol{H}_{\boldsymbol{\Lambda},u,1} & \\ & & \boldsymbol{H}_{\boldsymbol{\Lambda},u,-1} & \boldsymbol{H}_{\boldsymbol{\Lambda},u,0} & \boldsymbol{H}_{\boldsymbol{\Lambda},u,1} \end{bmatrix}$$

denote the equivalent channel between N_r-fold interpolated transmitted signal segment $\boldsymbol{s}'_{u,k}$ and received signal segment $\hat{\boldsymbol{y}}_{u,k}$. Notice that $\boldsymbol{H}_{\mathrm{eq}}$ is a Toeplitz matrix with $\boldsymbol{0}_{M\times 1}$ being its first column and $[0\ \cdots\ 0\ h_{L_H}\ \cdots\ h_{-L_H}\ 0\ \cdots\ 0]$ being its first row, where h_i is the ith tap coefficient of the equivalent channel, L_H is the length of causal and non-causal part of equivalent channel. Eq. (20) can be simplified as

$$\begin{aligned} \hat{\boldsymbol{y}}_{u,k} &= \boldsymbol{H}_{A,u}\left(\boldsymbol{I}_{(M_{b,u}+2L_{h,u})} \otimes \boldsymbol{e}_1\right)\boldsymbol{s}^o_{u,k} + \tilde{\boldsymbol{z}}_{u,k} \\ &= \sum_{i=-1}^{1} \boldsymbol{T}_{u,i}\underline{\boldsymbol{s}}_{u,k+i} + \tilde{\boldsymbol{z}}_{u,k}, \end{aligned} \tag{21}$$

where

$$\boldsymbol{H}_{A,u} = \boldsymbol{H}_{\mathrm{eq},u}\begin{bmatrix} \boldsymbol{0}_{(N-L-L_H)\times(M+2L_H)} \\ \boldsymbol{I}_{(M+2L_H)\times(M+2L_H)} \\ \boldsymbol{0}_{(N-L-L_H)\times(M+2L_H)} \end{bmatrix}, \tag{22}$$

$L_{h,u} = L_H/N_{r,u}$, $\boldsymbol{s}^o_{u,k}$ is the middle $M_b + 2L_{h,u}$ samples of successive blocks from $\boldsymbol{s}_{k-2}$ to $\boldsymbol{s}_{k+2}$, $\underline{\boldsymbol{s}}_k = \boldsymbol{P}_b[\boldsymbol{s}_{k-1}^{\mathrm{T}}\ \boldsymbol{s}_k^{\mathrm{T}}\ \boldsymbol{s}_{k+1}^{\mathrm{T}}]^{\mathrm{T}}$, $\underline{\boldsymbol{s}}_{k-1} = [\boldsymbol{0}_{L_h\times N_b-L_b-L_h}\ \boldsymbol{I}_{L_h}\ \boldsymbol{0}_{(L_h)\times L_b}]\boldsymbol{s}_{k-1}$, $\underline{\boldsymbol{s}}_{k+1} = [\boldsymbol{0}_{L_h\times L_b}\ \boldsymbol{I}_{L_h}\ \boldsymbol{I}_{L_h\times N_b-L_b-L_h}]\boldsymbol{s}_{k+1}$, $\boldsymbol{T}_{u,0}$ is given by

$$\boldsymbol{T}_{u,0} = \boldsymbol{H}_{M,u}\boldsymbol{W}_M^{\mathrm{H}}\boldsymbol{E}_u\boldsymbol{W}_{M_{b,u}}, \tag{23}$$

where $\boldsymbol{H}_{M,u} = \boldsymbol{H}_{A,u}[\boldsymbol{0}_{M\times L_H}\ \boldsymbol{I}_M\ \boldsymbol{0}_{M\times L_H}]^{\mathrm{T}}$. It should be noted that $\boldsymbol{H}_{A,u}$ is a $M \times (M + 2L_H)$ Toeplitz matrix with $[h_{L_H}\ 0\ \cdots\ 0]^{\mathrm{T}}$ being its first column and $[h_{L_H}\ \cdots\ h_{-L_H}\ 0\ \cdots\ 0]$ being its first row. $\boldsymbol{H}_A$ can be regarded as the effective channel with non-causal impulse response. $\boldsymbol{H}_M$ is a Toeplitz matrix with $[h_0\ \cdots\ h_{L_H}\ 0\ \cdots\ 0]^{\mathrm{T}}$ being the first column and $[h_0\ \cdots\ h_{-L_H}\ 0\ \cdots\ 0]$ being the first row.

As Figure 2 shows, linear equalizer needs be added to eliminate ISI. The matrix form of receiver is given as follows:

$$\hat{\mathbf{s}}_{u,k} = \boldsymbol{Q}_b\boldsymbol{W}_{M_{b,u}}^{\mathrm{H}}\boldsymbol{E}^{\mathrm{T}}\boldsymbol{\Lambda}_u^{\mathrm{H}}\boldsymbol{\Omega}_u\boldsymbol{W}_M\boldsymbol{y}_{u,k}, \tag{24}$$

where $\boldsymbol{\Omega}_u$ denotes equalizer of the uth UE. $\boldsymbol{\Omega}_u$ can be approximated to diagonal matrix [25]. Thus, the equalization and filter process can be merged without additional complexity. The frequency domain equalizer can be achieved by fast convolution filter banks with low complexity. In addition, FCMC based FDMA system brings another benefit that equalizations can be implemented in each subband without dependency and synchronization requirements.

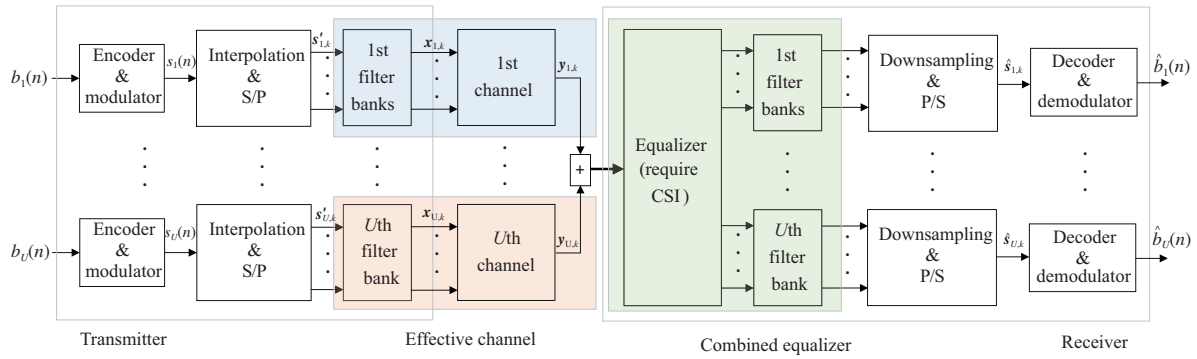

Figure 2 (Color online) FCMC transceiver processing flow in uplink transmission

3 Filtering design in frequency domain

In the proposed FCMC based FDMA transceiver, the pulse-shaping filtering is realized in the frequency domain, where frequency domain windowing is defined by a very low number of weight coefficients. By configuring rolloff factors and filter coefficients, frequency domain filters can reduce interference between adjacent subbands. However, since the frequency domain filter of each UE is band-limited, the designed filter may have a long impulse response which causes severe ISI. In order to ensure that transmission is free of ISI within subband as well as free of inter band interference (IBI), filter characteristics have to satisfy perfect reconstruction constraints in the assumption of ideal channel [27].

Substituting (18) into (12), we can write $\hat{\boldsymbol{s}}_{u,k}$ under the assumption of ideal channel conditions in the form as follows:

$$\hat{\boldsymbol{s}}_{u,k} = \sum_{u'=1}^{U} \sum_{k'=-2}^{2} \boldsymbol{\Theta}_{k',u,u'}(\boldsymbol{\Lambda}_u) \boldsymbol{s}_{u',k+k'}, \tag{25}$$

where $\boldsymbol{\Theta}_{k',u,u'}(\boldsymbol{\Lambda}_u)$ represents the influence on the kth unoverlapped block of the uth UE from $(k+k')$th block of the u'th UE. $\boldsymbol{\Theta}_{k',u,u}(\boldsymbol{\Lambda}_u)$ can be written as

$$\boldsymbol{\Theta}_{k',u,u'}(\boldsymbol{\Lambda}_u) = \boldsymbol{A}_u \boldsymbol{\Lambda}_u \tilde{\boldsymbol{C}}_{k',u'}(\boldsymbol{\Lambda}_u), \tag{26}$$

where $\boldsymbol{A}_u = \boldsymbol{Q}_{b,u} \boldsymbol{W}_{M_{b,u}}^{\mathrm{H}} \boldsymbol{E}_u^{\mathrm{T}}$, $\tilde{\boldsymbol{C}}_{k',u}$ is given as (19) with $\boldsymbol{H} = \boldsymbol{I}_{3N}$.

The perfect reconstruction (PR) condition in FCMC system can be written as

$$\boldsymbol{\Theta}_{k',u,u'} = \begin{cases} \boldsymbol{I}_{N_{b,u}}, & k' = 0, u = u', \\ \boldsymbol{0}_{N_{b,u}}, & \text{otherwise.} \end{cases} \tag{27}$$

For PR systems, the criterion for the prototype filter is very strict. In many practical applications, the PR property can be slightly relaxed, resulting in NPR systems. In these systems, the above-mentioned PR conditions only be met approximately. Thus, the NPR optimized filter banks in multiple subbands FCMC system should satisfy [19, 28]

$$\begin{aligned} &\arg\min_{\boldsymbol{\Lambda}_u} \quad ||\boldsymbol{\Theta}_{0,u,u} - \boldsymbol{I}_{N_{b,u}}||_F^2 + \sum_{k' \neq 0} ||\boldsymbol{\Theta}_{k',u,u}||_F^2 \\ &\text{s.t.} \quad \mathrm{Tr}(\boldsymbol{\Lambda}_u^{\mathrm{H}} \boldsymbol{\Lambda}_u) = M_{b,u}, \quad [\boldsymbol{\lambda}_u]_m = 0, \text{ for } m \notin \mathcal{I}_u, \end{aligned} \tag{28}$$

where $\mathcal{I}_u$ denotes subcarriers set occupied by the uth subband. Coefficients of subcarriers belonging to $\mathcal{I}_u$ are optimized, and subcarriers out of constrained bandwidth are trivial for the uth subband, i.e., $[\boldsymbol{\lambda}_u]_m = 0, \forall m \notin \mathcal{I}_u$. The optimization objective can be considered as minimizing in-band interference under filter energy and subcarriers range constraints. Since filter banks with different center frequencies can be obtained by a single low-pass subband filter shifting in the frequency domain, we simplify this optimization problem by considering a single-band system. For simplicity, we ignore subscript u in the

following. With vec-operator applied on the matrix $\boldsymbol{\Theta}_{k'}$, Eq. (28) can be rewritten as

$$\begin{aligned} &\arg\min_{\boldsymbol{\Lambda}} \quad \|\tilde{\boldsymbol{\Theta}}_0 - \mathrm{vec}(\boldsymbol{I}_{N_b})\|_2^2 + \sum_{k'\neq 0} \|\tilde{\boldsymbol{\Theta}}_{k'}\|_2^2 \\ &\text{s.t.} \quad \mathrm{Tr}(\boldsymbol{\Lambda}^{\mathrm{H}}\boldsymbol{\Lambda}) = M_b, \quad [\boldsymbol{\lambda}]_m = 0, \text{ for } m \notin \mathcal{I}, \end{aligned} \tag{29}$$

where $\tilde{\boldsymbol{\Theta}}_k = \mathrm{vec}(\boldsymbol{\Theta}_k)$.

Let

$$\boldsymbol{D}_i = \boldsymbol{W}_M \boldsymbol{P}_i \boldsymbol{Q} \boldsymbol{W}_M^{\mathrm{H}}, \quad i = -1, 0, 1, \tag{30}$$

$$\boldsymbol{B}_j = \boldsymbol{E}\boldsymbol{W}_{M_b} \boldsymbol{P}_{b,j}, \quad j = -1, 0, 1, \tag{31}$$

then $\mathrm{vec}(\boldsymbol{A}\boldsymbol{\Lambda}\boldsymbol{D}_i\boldsymbol{\Lambda}\boldsymbol{B}_j)$ can be written as

$$\mathrm{vec}(\boldsymbol{A}\boldsymbol{\Lambda}\boldsymbol{D}_i\boldsymbol{\Lambda}\boldsymbol{B}_j) = (\boldsymbol{B}_j^{\mathrm{T}} \otimes \boldsymbol{A})\tilde{\boldsymbol{D}}_i(\boldsymbol{\lambda} \otimes \boldsymbol{\lambda}), \tag{32}$$

where $\tilde{\boldsymbol{D}}_i = \mathrm{diag}\left(\mathrm{vec}\left(\boldsymbol{D}_i\right)\right)$. The mth element of $\mathrm{vec}(\boldsymbol{A}\boldsymbol{\Lambda}\boldsymbol{D}_i\boldsymbol{\Lambda}\boldsymbol{B}_j)$ can be written as

$$[\mathrm{vec}(\boldsymbol{A}\boldsymbol{\Lambda}\boldsymbol{D}_i\boldsymbol{\Lambda}\boldsymbol{B}_j)]_m = \boldsymbol{\lambda}^{\mathrm{T}}\boldsymbol{Y}_{i,j,m}\boldsymbol{\lambda}, \tag{33}$$

where $\mathrm{vec}\left(\boldsymbol{Y}_{i,j,m}\right) = \left([(\boldsymbol{B}_j^{\mathrm{T}} \otimes \boldsymbol{A})\tilde{\mathbf{D}}_i]_m\right)^{\mathrm{T}}$. Thus, Eq. (29) can be rewritten as

$$\arg\min_{\boldsymbol{\Lambda}_u} \|\underline{\tilde{\boldsymbol{\Theta}}}\|_2^2 \qquad \text{s.t.} \quad \mathrm{Tr}(\boldsymbol{\Lambda}^{\mathrm{H}}\boldsymbol{\Lambda}) = M_b, \quad [\boldsymbol{\lambda}]_m = 0, \text{ for } m \notin \mathcal{I}, \tag{34}$$

where $\underline{\tilde{\boldsymbol{\Theta}}} = [\underline{\tilde{\boldsymbol{\Theta}}}_{-2}^{\mathrm{T}}\ \underline{\tilde{\boldsymbol{\Theta}}}_{-1}^{\mathrm{T}}\ \underline{\tilde{\boldsymbol{\Theta}}}_{0}^{\mathrm{T}}\ \underline{\tilde{\boldsymbol{\Theta}}}_{1}^{\mathrm{T}}\ \underline{\tilde{\boldsymbol{\Theta}}}_{2}^{\mathrm{T}}]^{\mathrm{T}}$. $\underline{\tilde{\boldsymbol{\Theta}}}_i$ for $-2 \leqslant i \leqslant 2$ are defined as follows:

$$\begin{aligned} \left[\underline{\tilde{\boldsymbol{\Theta}}}_{-2}\right]_m &= \boldsymbol{\lambda}^{\mathrm{T}}\boldsymbol{Y}_{-1,-1,m}\boldsymbol{\lambda}, \\ \left[\underline{\tilde{\boldsymbol{\Theta}}}_{-1}\right]_m &= \boldsymbol{\lambda}^{\mathrm{T}}\left(\boldsymbol{Y}_{-1,0,m} + \boldsymbol{Y}_{0,-1,m}\right)\boldsymbol{\lambda}, \\ \left[\underline{\tilde{\boldsymbol{\Theta}}}_{0}\right]_m &= \begin{cases} \boldsymbol{\lambda}^{\mathrm{T}}(\boldsymbol{Y}_{0,0,m} + \boldsymbol{Y}_{-1,1,m} + \boldsymbol{Y}_{1,-1,m} - \frac{1}{N_a}\boldsymbol{I}_M)\boldsymbol{\lambda}, \text{ for } m = nM + n \text{ with } 1 \leqslant n \leqslant M, \\ \boldsymbol{\lambda}^{\mathrm{T}}\left(\boldsymbol{Y}_{0,0,m} + \boldsymbol{Y}_{-1,1,m} + \boldsymbol{Y}_{1,-1,m}\right)\boldsymbol{\lambda}, \text{ otherwise}, \end{cases} \\ \left[\underline{\tilde{\boldsymbol{\Theta}}}_{1}\right]_m &= \boldsymbol{\lambda}^{\mathrm{T}}\left(\boldsymbol{Y}_{1,0,m} + \boldsymbol{Y}_{0,1,m}\right)\boldsymbol{\lambda}, \\ \left[\underline{\tilde{\boldsymbol{\Theta}}}_{2}\right]_m &= \boldsymbol{\lambda}^{\mathrm{T}}\boldsymbol{Y}_{1,1,m}\boldsymbol{\lambda}. \end{aligned} \tag{35}$$

Let $\boldsymbol{\lambda}_t$ and $\boldsymbol{\lambda}_r$ denote transmitted and received frequency domain filter coefficients separately. $\boldsymbol{\lambda}_t$ and $\boldsymbol{\lambda}_r$ should satisfy the relationship that $\boldsymbol{\lambda}_t = \boldsymbol{\lambda}_r = \boldsymbol{\lambda}$. We alternately update $\boldsymbol{\lambda}_t$ and $\boldsymbol{\lambda}_r$ to satisfy optimization objective (34) and make $\boldsymbol{\lambda}_t$ and $\boldsymbol{\lambda}_r$ tend to be consistent.

When $\boldsymbol{\lambda}_t$ is fixed, the perfect reconstruction condition is transferred to the following least squares problem

$$\arg\min_{\boldsymbol{\lambda}_r} \quad ||\boldsymbol{F}^{(i)}\boldsymbol{\lambda}_r||_2^2 \qquad \text{s.t.} \quad \mathrm{Tr}(\boldsymbol{\lambda}_r^{\mathrm{T}}\boldsymbol{\lambda}_r) = M_b, \quad [\boldsymbol{\lambda}_r]_m = 0, \text{ for } m \notin \mathcal{I}, \tag{36}$$

where i denotes the ith iteration. $\boldsymbol{F}^{(i)}$ is $5N_b^2 \times N$ matrix given by

$$\boldsymbol{F}^{(i)} = \left[\left(\boldsymbol{F}_{-2}^{(i)}\right)^{\mathrm{T}}\ \left(\boldsymbol{F}_{-1}^{(i)}\right)^{\mathrm{T}}\ \left(\boldsymbol{F}_{0}^{(i)}\right)^{\mathrm{T}}\ \left(\boldsymbol{F}_{1}^{(i)}\right)^{\mathrm{T}}\ \left(\boldsymbol{F}_{2}^{(i)}\right)^{\mathrm{T}}\right]^{\mathrm{T}}, \tag{37}$$

where

$$\begin{aligned}
\left[\boldsymbol{F}_{-2}^{(i)}\right]_m &= \left(\boldsymbol{\lambda}_t^{(i)}\right)^{\mathrm{T}} \boldsymbol{Y}_{-1,-1,m},\\
\left[\boldsymbol{F}_{-1}^{(i)}\right]_m &= \left(\boldsymbol{\lambda}_t^{(i)}\right)^{\mathrm{T}} \left(\boldsymbol{Y}_{-1,0,m} + \boldsymbol{Y}_{0,-1,m}\right),\\
\left[\boldsymbol{F}_{0}^{(i)}\right]_m &= \begin{cases} \left(\boldsymbol{\lambda}_t^{(i)}\right)^{\mathrm{T}} \left(\boldsymbol{Y}_{0,0,m} + \boldsymbol{Y}_{-1,1,m} + \boldsymbol{Y}_{1,-1,m} - \frac{1}{N_a}\boldsymbol{I}_M\right), \text{ for } m{=}nM+n \text{ with } 1 \leqslant n \leqslant M,\\ \left(\boldsymbol{\lambda}_t^{(i)}\right)^{\mathrm{T}} \left(\boldsymbol{Y}_{0,0,m} + \boldsymbol{Y}_{-1,1,m} + \boldsymbol{Y}_{1,-1,m}\right), \text{ otherwise,} \end{cases}\\
\left[\boldsymbol{F}_{1}^{(i)}\right]_m &= \left(\boldsymbol{\lambda}_t^{(i)}\right)^{\mathrm{T}} \left(\boldsymbol{Y}_{1,0,m} + \boldsymbol{Y}_{0,1,m}\right),\\
\left[\boldsymbol{F}_{2}^{(i)}\right]_m &= \left(\boldsymbol{\lambda}_t^{(i)}\right)^{\mathrm{T}} \boldsymbol{Y}_{1,1,m}.
\end{aligned} \tag{38}$$

This LS problem can be solved by singular value decomposition (SVD). Let

$$\boldsymbol{F}_r^{(i)} = \left[\left(\mathrm{Re}(\boldsymbol{F}^{(i)})\right)^{\mathrm{T}} \left(\mathrm{Im}(\boldsymbol{F}^{(i)})\right)^{\mathrm{T}}\right]^{\mathrm{T}}, \tag{39}$$

then, find the SVD of $\boldsymbol{F}_r^{(i)}(\boldsymbol{F}_r^{(i)})^{\mathrm{T}}$ as follows:

$$\boldsymbol{F}_r^{(i)} \left(\boldsymbol{F}_r^{(i)}\right)^{\mathrm{T}} = \mathbf{U}\boldsymbol{\Sigma}\mathbf{U}^{\mathrm{T}}. \tag{40}$$

The optimal $\boldsymbol{\lambda}_r^{(i+1)}$ is the right singular vector of the minimum eigenvalue.

We iteratively update $\boldsymbol{\lambda}_t$ to approach $\boldsymbol{\lambda}_r$ until $||\boldsymbol{\lambda}_t - \boldsymbol{\lambda}_r||_2 < \epsilon$ with ϵ being the error tolerance between $\boldsymbol{\lambda}_t$ and $\boldsymbol{\lambda}_r$. $\boldsymbol{\lambda}_t$ is updated as

$$\boldsymbol{\lambda}_t^{(i+1)} = \beta\boldsymbol{\lambda}_t^{(i)} + (1-\beta)\boldsymbol{\lambda}_r^{(i+1)}, \tag{41}$$

where β is the weighting factor for trading between $\boldsymbol{\lambda}_t^{(i)}$ and $\boldsymbol{\lambda}_r^{(i+1)}$.

In this contribution, we propose the NPR filter bank design method in FCMC system by minimizing reconstruction error under filter energy and subband subcarriers range constraints. When $\boldsymbol{\lambda}_t$ is fixed, $\boldsymbol{\lambda}_r$ is optimized by minimizing the reconstruction error. This optimization problem is converted to LS problem shown in (36). $\boldsymbol{\lambda}_t$ is updated as (41). Through alternately updating $\boldsymbol{\lambda}_t$ and $\boldsymbol{\lambda}_r$, the gap between them decreases, and $\boldsymbol{\lambda}_t$ can be seen as the optimal filter bank. The proposed filter optimization algorithm is shown in Algorithm 1.

Algorithm 1 Proposed FC-FB optimization algorithm

Require: Subcarriers number of the uth subband: $N_{a,u}$; bandwidth of the uth subband: $M_{b,u}$; the allowed maximum error between optimized transmitted and received filter bank: ϵ; $\boldsymbol{\lambda}_t^{(0)}$ and $\boldsymbol{\lambda}_r^{(0)}$ as RRC filters which satisfies subband bandwidth $M_{b,u}$ and subcarrier number $N_{a,u}$ constraints.

Ensure: The optimized transmitted and received filter bank: $\boldsymbol{\lambda}$.

1: **while** $||\boldsymbol{\lambda}_t - \boldsymbol{\lambda}_r||_2 > \epsilon$ **do**
2: Fix $\boldsymbol{\lambda}_t$, calculate $\boldsymbol{F}$ by (37).
3: Let $\boldsymbol{F}_r = [(\mathrm{Re}(\boldsymbol{F}))^{\mathrm{T}}\ (\mathrm{Im}(\boldsymbol{F}))^{\mathrm{T}}]^{\mathrm{T}}$. Find SVD of $\boldsymbol{F}_r\boldsymbol{F}_r^{\mathrm{T}}$, and the corresponding right singular vector of minimum positive eigenvalue is the optimized $\boldsymbol{\lambda}_r^{(i)}$ with fixed $\boldsymbol{\lambda}_t^{(i-1)}$.
4: Update $\boldsymbol{\lambda}_t$: $\boldsymbol{\lambda}_t^{(i)} = \beta\boldsymbol{\lambda}_t^{(i-1)} + (1-\beta)\boldsymbol{\lambda}_r^{(i)}$.
5: **end while**
6: Set $\boldsymbol{\lambda} = \boldsymbol{\lambda}_t^{(i)}$.
7: **return** $\boldsymbol{\lambda}$.

4 Low-complexity frequency domain equalizer

In this section, we investigate the one-tap equalizer based on FC-FB. Assume the receiver can exploit extra CSI to permit equalization. We consider a single-band system in this section, and it is convenient to apply the proposed one-tap equalizers to FCMC based FDMA system with multiple subbands.

4.1 FC-MMSE one-tap equalizer

It was demonstrated that equalizer $\boldsymbol{\Omega}$ in (24) can be simplified to one-tap equalizer [25], i.e., $\boldsymbol{\Omega} = \mathrm{diag}\,(\boldsymbol{\omega})$. The equalization and matched filter process can be merged without additional complexity. Thus, we can consider designing the combined equalizer, and the equalized channel is the combination of the physical channel and the synthesis filter banks. We view the frequency selective channel between modulated interpolated signal and received signal as effective channel shown in Figure 2.

Different from the design of filter banks, the equalizer is optimized only in the receiver side. Thus, $\hat{\underline{\boldsymbol{s}}}_k$ can be written as

$$\hat{\underline{\boldsymbol{s}}}_{u,k} = \underline{\boldsymbol{A}}_u \boldsymbol{\Omega}_u \boldsymbol{y}_{u,k}^f, \tag{42}$$

where $\underline{\boldsymbol{A}}_u = \boldsymbol{W}_{M_{b,u}}^{\mathrm{H}} \boldsymbol{E}^{\mathrm{T}}$. The above equation indicates the linear relationship between $\hat{\underline{\mathbf{s}}}_{u,k}$ and $\boldsymbol{\Omega}_u$. With the MMSE criterion, $\boldsymbol{\Omega}$ is required to satisfy

$$\arg\min_{\boldsymbol{\Omega}} \mathrm{E}\left\{ \left\| \underline{\boldsymbol{A}} \boldsymbol{\Omega} \boldsymbol{y}_k^f - \underline{\boldsymbol{s}}_k \right\|_2^2 \right\}, \tag{43}$$

where $\underline{\boldsymbol{A}} = \boldsymbol{W}_{M_b}^{\mathrm{H}} \boldsymbol{E}^{\mathrm{T}}$. Calculate the derivative of expectation with respect to $\boldsymbol{\omega}$ and set it to 0 as

$$\frac{\partial \mathrm{E}\{\|\underline{\mathbf{A}} \boldsymbol{\Omega} \boldsymbol{y}_k^f - \underline{\boldsymbol{s}}_k\|_2^2\}}{\partial \boldsymbol{\omega}^{\mathrm{H}}} = \mathrm{E}\{\boldsymbol{Y}_k^{\mathrm{H}} \underline{\boldsymbol{A}}^{\mathrm{H}} \underline{\boldsymbol{A}} \boldsymbol{Y}_k\} \boldsymbol{\omega} - \mathrm{E}\{\boldsymbol{Y}_k^{\mathrm{H}} \underline{\boldsymbol{A}}^{\mathrm{H}} \underline{\boldsymbol{s}}_k\} = 0, \tag{44}$$

where $\boldsymbol{Y}_k$ is $M \times M$ diagonal matrix with $\hat{\boldsymbol{y}}_k^f$ on its diagonal. Thus, substituting (21) into (44), we find the optimal $\boldsymbol{\omega}$ should meet the condition as

$$\begin{aligned}
\hat{\boldsymbol{\omega}} =& \left(\mathrm{E}\{\boldsymbol{Y}_k^{\mathrm{H}} \underline{\boldsymbol{A}}^{\mathrm{H}} \underline{\boldsymbol{A}} \boldsymbol{Y}_k\} \right)^{-1} \mathrm{E}\{\boldsymbol{Y}_k^{\mathrm{H}} \underline{\boldsymbol{A}}^{\mathrm{H}} \underline{\boldsymbol{s}}_k\} \\
=& \left(\mathrm{E}\left\{ \left(\hat{\boldsymbol{y}}_k^f \right)^{\mathrm{H}} \hat{\boldsymbol{y}}_k^f \right\}^* \odot \underline{\boldsymbol{A}}^{\mathrm{H}} \underline{\boldsymbol{A}} \right) \left(\mathrm{E}\left\{ \hat{\boldsymbol{y}}_k^f \boldsymbol{s}_k^{\mathrm{H}} \right\}^* \odot \underline{\boldsymbol{A}}^{\mathrm{H}} \right) \mathbf{1} \\
=& \left(\left(\sum_{i=-1}^{1} \boldsymbol{W}_M \boldsymbol{T}_i \boldsymbol{T}_i^{\mathrm{H}} \boldsymbol{W}_M^{\mathrm{H}} + \sigma^2 \boldsymbol{I}_M \right)^* \odot \left(\underline{\boldsymbol{A}}^{\mathrm{H}} \underline{\boldsymbol{A}} \right) \right)^{-1} \left((\boldsymbol{W}_M \boldsymbol{T}_0)^* \odot \underline{\boldsymbol{A}}^{\mathrm{H}} \right) \mathbf{1},
\end{aligned} \tag{45}$$

where σ^2 denotes noise variance. Eq. (45) represents the one-tap frequency domain equalizer based on the MMSE criterion in the FCMC system.

Although the one-tap frequency domain equalizer can be implemented with low complexity by fast convolution filter banks, the calculation of the one-tap equalizer coefficients in (45) is relatively complicated due to the high computational complexity of matrix inverse. In the next section, we would take some approximations to further simplify the calculation.

4.2 FC-MMSE low-complexity one-tap equalizer

When the frequency selectivity of the combined channel is less serious, i.e., $h_i \gg h_{i+N_s}$ for $1 \leqslant i \leqslant N_s$, $\boldsymbol{T}_{-1}$ and $\boldsymbol{T}_1$ can be ignored compared to $\boldsymbol{T}_0$. From (21), we can see that $\hat{\boldsymbol{y}}_k$ is irrelevant to $\underline{\boldsymbol{s}}_{k-1}$ and $\underline{\boldsymbol{s}}_{k+1}$. Note that the combined CIR is the convolution of the physical CIR and the filter impulse response. Since the synthesis filter bank is optimized, the filter impulse response has shorter tails. The combined CIR can always satisfy the above conditions for most physical channel models. The equalizer can be simplified to

$$\hat{\boldsymbol{\omega}} = \left(\left(\boldsymbol{W}_M \boldsymbol{T}_0 \boldsymbol{T}_0^{\mathrm{H}} \boldsymbol{W}_M^{\mathrm{H}} + \sigma^2 \boldsymbol{I}_M \right)^* \odot \left(\underline{\boldsymbol{A}}^{\mathrm{H}} \underline{\boldsymbol{A}} \right) \right)^{-1} \left((\boldsymbol{W}_M \boldsymbol{T}_0)^* \odot \underline{\boldsymbol{A}}^{\mathrm{H}} \right) \mathbf{1}. \tag{46}$$

We study the asymptotic eigenvalue distribution of Toeplitz matrices and prove that $\boldsymbol{H}_M$ can be asymptotically diagonalized by $\boldsymbol{W}_M$ using lemmas in [25, 29].

Lemma 1. Given two $M \times M$ matrices $\boldsymbol{G}$ and $\boldsymbol{H}$. We have

$$\|\boldsymbol{G}\boldsymbol{H}\|_F \leqslant \|\boldsymbol{G}\|_2 \cdot \|\boldsymbol{H}\|_2, \tag{47}$$

and

$$\|\boldsymbol{G}\boldsymbol{H}\|_F \leqslant \|\boldsymbol{G}\|_F \cdot \|\boldsymbol{H}^{\mathrm{H}}\|_2. \tag{48}$$

Lemma 2. Given a Toeplitz matrix $\boldsymbol{T}_M$ and a circulant matrix $\boldsymbol{C}_M$ generated by the first column of $\boldsymbol{T}_M$, they are asymptotically equivalent, i.e.,

$$\lim_{M\to\infty} \|\boldsymbol{T}_M - \boldsymbol{C}_M\|_F = 0. \tag{49}$$

Theorem 1. Toeplitz matrix $\boldsymbol{T}_M$ is asymptotically diagonalized by $\boldsymbol{W}_M$ as $\boldsymbol{\Lambda}_M$ [25], i.e.,

$$\lim_{M\to\infty} \|\boldsymbol{W}_M \boldsymbol{T}_M \boldsymbol{W}_M^{\mathrm{H}} - \boldsymbol{\Lambda}_M\|_F = 0. \tag{50}$$

Proof. Define the circulant matrix $\boldsymbol{C}_M$ and $\boldsymbol{R}_M = \boldsymbol{T}_M - \boldsymbol{C}_M$, thus $\lim_{M\to\infty} \|\boldsymbol{R}_M\|_F = 0$. Define the diagonalized circulant matrix as $\boldsymbol{\Lambda}_M = \boldsymbol{W}_M^{\mathrm{H}} \boldsymbol{C}_M \boldsymbol{W}_M$, then

$$\boldsymbol{W}_M \boldsymbol{T}_M \boldsymbol{W}_M^{\mathrm{H}} - \boldsymbol{\Lambda}_M = \boldsymbol{W}_M \boldsymbol{R}_M \boldsymbol{W}_M^{\mathrm{H}}. \tag{51}$$

According to Lemma 1, we have

$$\|\boldsymbol{W}_M \boldsymbol{R}_M \boldsymbol{W}_M^{\mathrm{H}}\|_F \leqslant \|\boldsymbol{R}_M\|_F. \tag{52}$$

Hence $\lim_{M\to\infty} \|\boldsymbol{W}_M \boldsymbol{T}_M \boldsymbol{W}_M^{\mathrm{H}} - \boldsymbol{\Lambda}_M\|_F = 0$.

In practice, $M = 2048$ is good enough for approximation. Thus, $\boldsymbol{H}_M$ can be asymptotically diagonalized by DFT and IDFT matrices as follows:

$$\lim_{M\to\infty} \|\boldsymbol{W}_M \boldsymbol{H}_M \boldsymbol{W}_M^{\mathrm{H}} - \boldsymbol{H}_f\|_F = 0. \tag{53}$$

Substituting (53) into (46), we get

$$\hat{\boldsymbol{\omega}} = \left(\left(\boldsymbol{H}_f \underline{\boldsymbol{A}}^{\mathrm{H}} \underline{\boldsymbol{A}} \boldsymbol{H}_f^{\mathrm{H}} + \sigma^2 \boldsymbol{I}_M\right)^* \odot \left(\underline{\boldsymbol{A}}^{\mathrm{H}} \underline{\boldsymbol{A}}\right)\right)^{-1} \left(\left(\boldsymbol{H}_f \underline{\boldsymbol{A}}^{\mathrm{H}}\right)^* \odot \underline{\boldsymbol{A}}^{\mathrm{H}}\right) \mathbf{1}. \tag{54}$$

The equalizer above can be simplified to

$$\hat{\boldsymbol{\omega}} = \left(\boldsymbol{H}_f \mathbf{E}\mathbf{E}^{\mathrm{T}} \boldsymbol{H}_f^{\mathrm{H}} + \sigma^2 \boldsymbol{I}_M\right)^{-1} \mathrm{diag}\left(\boldsymbol{H}_f^{\mathrm{H}}\right). \tag{55}$$

Combining the one-tap equalizer and downsampling filter, we get

$$\boldsymbol{\Omega}' = \boldsymbol{E}^{\mathrm{T}} \boldsymbol{\Omega} = \left(\boldsymbol{E}^{\mathrm{T}} \boldsymbol{H}_f^{\mathrm{H}} \boldsymbol{H}_f \boldsymbol{E} + \sigma^2 \boldsymbol{I}_{M_b}\right)^{-1} \boldsymbol{E}^{\mathrm{T}} \boldsymbol{H}_f^{\mathrm{H}}, \tag{56}$$

where $\boldsymbol{E}^{\mathrm{T}} \boldsymbol{H}_f^{\mathrm{H}} \boldsymbol{H}_f \boldsymbol{E} + \sigma^2 \boldsymbol{I}_{M_b}$ is a diagonal matrix making the matrix inverse simpler. Thus, from the fact that Toeplitz matrices can be asymptotically diagonalized by DFT matrix, the channel equalizer can be simplified to one-tap frequency domain equalizer shown in (56) reasonably when DFT size is large enough in channel with less severe frequency selectivity. Hence, the computational complexity of equalizer is greatly reduced.

Now FCMC receiver with equalizer can be derived according to (24) and (56) as

$$\hat{\mathbf{s}}_{u,k} = \boldsymbol{Q}_b \boldsymbol{W}_{M_{b,u}}^{\mathrm{H}} \left(\boldsymbol{E}^{\mathrm{T}} \boldsymbol{H}_f^{\mathrm{H}} \boldsymbol{H}_f \boldsymbol{E} + \sigma^2 \boldsymbol{I}_{M_b}\right)^{-1} \boldsymbol{E}^{\mathrm{T}} \boldsymbol{H}_f^{\mathrm{H}} \boldsymbol{W}_M \boldsymbol{y}_{u,k}. \tag{57}$$

5 Pilot design and channel estimation

In order to acquire effective CSI required by frequency domain equalizer, we investigate the frequency domain effective channel estimation method with pilot assistance. Since the frequency domain pilots insertion destroys FC-FBs implementation, the spectral leakage cannot be suppressed by filter banks. High interference is brought between adjacent subbands. On the contrary, the time domain pilots insertion does not induce destruction of transmitted signal power spectrum. In this section, we propose time domain pilots design and effective channel estimation method.

5.1 Pilot design

In the time domain, pilots and data segments are placed alternately. Note that the time interval between adjacent pilot segments should be longer than coherence time. Zadoff-Chu (ZC) sequences with ideal auto-correlation and good cross-correlation properties are given as follows:

$$p^r(n) = \exp\left(\mathrm{j}\pi \frac{rn(n+(N)_2+2qN)}{N}\right), \quad 0 < n < N-1, \tag{58}$$

where $p^r(n)$ denotes the N-points ZC sequence with root r for any integer q. Set $q = 0$. r satisfies the condition that $0 < r < N$, and r is relatively prime to N.

We first consider a single-subband FCMC system for channel estimation. Let

$$\boldsymbol{p} = \Big[p(0), \ldots, p(N_{p,b}-1)\Big]^{\mathrm{T}}, \tag{59}$$

where $N_{p,b}$ denotes the length of pilot segment, $p(n)$ denotes the nth coefficient of the pilot segment. Suppose $\boldsymbol{s}_l$ and $\boldsymbol{s}_r$ are the last and the next data segment of pilot. Received pilot can be derived according to (20) as

$$\boldsymbol{y}_p = \boldsymbol{H}_p\left(\boldsymbol{I}_{N_{p,b}+2L_h} \otimes \boldsymbol{e}_1\right)\boldsymbol{p}' + \boldsymbol{z}_p, \tag{60}$$

where $\boldsymbol{H}_p$ is $N_p \times (N_p + 2L_H)$ Toeplitz matrix with $[h_{L_H}\ 0\ \cdots\ 0]^{\mathrm{T}}$ and $[h_{L_H}\ \cdots\ h_{-L_H}\ 0\ \cdots\ 0]^{\mathrm{T}}$ being its first column and first row, $N_p = N_r N_{p,b}$, $\boldsymbol{p}'$ is the middle $N_{p,b} + 2L_h$ points of $[\,\boldsymbol{s}_l^{\mathrm{T}}\ \boldsymbol{p}^{\mathrm{T}}\ \boldsymbol{s}_r^{\mathrm{T}}\,]^{\mathrm{T}}$.

From (60), we can see that ISI is induced to the received signal blocks due to effective frequency-selective channel. With CP insertion in OFDM transmission system, linear convolution between data block and channel impulse response (CIR) can be transformed to circular convolution between data block with CP discarded and CIR. When CP length is longer than CIR, interference from adjacent symbols is eliminated. As non-causal filter banks are applied in FCMC based FDMA system, the proposed combined CP and CS pilot structure is written as

$$\boldsymbol{p}^* = \Big[\,\boldsymbol{p}_{s,\mathrm{CP}}^{\mathrm{T}}\ \boldsymbol{p}_s^{\mathrm{T}}\ \boldsymbol{p}_{s,\mathrm{CS}}^{\mathrm{T}}\,\Big]^{\mathrm{T}}, \tag{61}$$

where $\boldsymbol{p}_s$ of size N_{ps} denotes effective pilot, CP and CS are given by

$$\boldsymbol{p}_{s,\mathrm{CP}} = \Big[\,\boldsymbol{0}_{N_{\mathrm{CP}}\times(N_{\mathrm{ps}}-N_{\mathrm{CP}})}\ \boldsymbol{I}_{N_{\mathrm{CP}}}\,\Big]\boldsymbol{p}_s, \tag{62}$$

$$\boldsymbol{p}_{s,\mathrm{CS}} = \Big[\,\boldsymbol{I}_{N_{\mathrm{CS}}}\ \boldsymbol{0}_{N_{\mathrm{CS}}\times(N_{\mathrm{ps}}-N_{\mathrm{CS}})}\,\Big]\boldsymbol{p}_s. \tag{63}$$

Length of CP and CS should be longer than time spread of causal and anti-causal part in joint channel in order to eliminate interferences between adjacent blocks. It should be noted that the CP and CS are added as part of the pilot. Since the pilot occupies a small part of the frame structure, the proposed combined CP and CS pilot structure only slightly decreases the spectral efficiency compared with FBMC.

5.2 Single subband channel estimation with designed pilot

The time domain CSI obtained by traditional time domain channel estimation cannot be directly used for frequency domain equalization in FCMC based FDMA system. In this part, we investigate the frequency domain effective CSI estimation method with the pilot in combined CP and CS structure.

Substituting (61) into (60), the received pilot can be reformulated as

$$\boldsymbol{y}_{p^*} = \boldsymbol{\Psi}\boldsymbol{R}\boldsymbol{G}\boldsymbol{h} + \boldsymbol{z}_p, \tag{64}$$

where $\boldsymbol{h} = [h_0\ \cdots\ h_{L_H}\ 0\ \cdots\ 0\ h_{-L_H}\ \cdots\ h_{-1}]^{\mathrm{T}}$ of length M denotes impulse response of effective channel, $\boldsymbol{G}$ is given by

$$\boldsymbol{G} = \begin{bmatrix} \boldsymbol{I}_{\frac{N_p}{2}} & \boldsymbol{0}_{\frac{N_p}{2}\times(M-N_p)} & \boldsymbol{0}_{\frac{N_p}{2}} \\ \boldsymbol{0}_{\frac{N_p}{2}} & \boldsymbol{0}_{\frac{N_p}{2}\times(M-N_p)} & \boldsymbol{I}_{\frac{N_p}{2}} \end{bmatrix}^{\mathrm{T}}, \tag{65}$$

$\boldsymbol{R}$ is 1-offset circular shift permutation matrix and given by

$$\boldsymbol{R}_{i,j} = \begin{cases} 1, & \text{if } j = (i+1) \bmod N_p, \\ 0, & \text{otherwise.} \end{cases} \tag{66}$$

$\boldsymbol{\Psi}$ is a circulant matrix with $\left(\boldsymbol{I}_{N_{p,b}} \otimes \boldsymbol{e}_1\right) \boldsymbol{p}_s^r$ being its first column and can be diagonalized by DFT matrix $\boldsymbol{W}_{N_p}$ as follows:

$$\boldsymbol{\Psi} = \boldsymbol{W}_{N_p}^{\mathrm{H}} \boldsymbol{\Phi} \boldsymbol{W}_{N_p}, \tag{67}$$

where $\mathrm{diag}\,(\boldsymbol{\Phi}) = \boldsymbol{W}_{N_p}(\boldsymbol{I}_{N_{p,b}} \otimes \boldsymbol{e}_1)\boldsymbol{p}_s^r$ with $\boldsymbol{p}_s^r$ represents $\boldsymbol{p}_s$ in reverse order.

Based on (60), LS estimation of $\boldsymbol{h}$ can be written as

$$\hat{\boldsymbol{h}} = \boldsymbol{G}^{\mathrm{T}} \boldsymbol{R}^{\mathrm{T}} \boldsymbol{W}_{N_p}^{\mathrm{H}} \boldsymbol{\Phi}^{\mathrm{H}} \boldsymbol{W}_{N_p} \boldsymbol{y}_{p^*}. \tag{68}$$

Frequency domain channel can be obtained by taking DFT of joint CIR as

$$\hat{\boldsymbol{H}}_f = \boldsymbol{W}_M \hat{\boldsymbol{h}}. \tag{69}$$

Combining (68) and (69), we get

$$\hat{\boldsymbol{H}}_f = \boldsymbol{W}_M \boldsymbol{G}^{\mathrm{T}} \boldsymbol{R}^{\mathrm{T}} \boldsymbol{W}_{N_p}^{\mathrm{H}} \boldsymbol{\Phi}^{\mathrm{H}} \boldsymbol{W}_{N_p} \boldsymbol{y}_{p^*}. \tag{70}$$

Eq. (70) gives an approach of effective channel estimation based on time domain pilot in FCMC system.

Let $N_p = M$, then the frequency domain CSI estimator (70) can be simplified to

$$\hat{\boldsymbol{H}}_f = \boldsymbol{\Phi}^{\mathrm{H}} \boldsymbol{W}_M \boldsymbol{R}^{\mathrm{T}} \boldsymbol{y}_{p^*}. \tag{71}$$

Notice that $\boldsymbol{\Phi}$ is diagonal, the channel estimator can be realized with low complexity when pilot length is M_b.

With the assistance of pilots in the proposed structure shown in (61), the interference between the pilot segment and the adjacent data segment can be removed. Without the aid of CP and CS, the received pilot cannot be transformed to the circular convolution of the interpolated transmitted pilot and the effective CIR. Thus, the proposed channel estimation scheme is not effective without CP and CS in pilot structure. As shown in (71), the proposed channel estimation method is composed of three steps: (a) taking circular shift of received pilot signal; (b) transforming to frequency domain by M-points FFT; (c) taking dot product between frequency signal and diag($\boldsymbol{\Phi}^{\mathrm{H}}$). Thus the complexity of the proposed CSI estimation method assisted with pilots in the combined CP and CS structure is relatively low.

5.3 Channel estimation with multiple UEs

When multiple UEs exists in the system, the received pilot signal can be written as

$$\hat{\boldsymbol{y}}_{p^*,u} = \sum_{u=1}^{U} \boldsymbol{\Psi}_u \boldsymbol{R} \boldsymbol{G} \boldsymbol{h}_u + \boldsymbol{z}_p, \tag{72}$$

where $\boldsymbol{z}_p = \sum_{u=1}^{U} \boldsymbol{z}_{p,u}$. Substituting (71) into (72), we get

$$\hat{\boldsymbol{H}}_{f,u} = \boldsymbol{H}_{f,u} + \sum_{u' \neq u} \boldsymbol{R}^{\mathrm{T}} \boldsymbol{\Phi}_u^{\mathrm{H}} \boldsymbol{\Phi}_{u'} \boldsymbol{R} \boldsymbol{H}_{f,u'} + \boldsymbol{z}_u^{\mathrm{LS}}. \tag{73}$$

The estimation error for the uth UE is

$$\begin{aligned} \boldsymbol{e}_u^{\mathrm{LS}} =& \hat{\boldsymbol{H}}_{f,u} - \boldsymbol{H}_{f,u} \\ =& \sum_{u' \neq u} \boldsymbol{R}^{\mathrm{T}} \boldsymbol{\Phi}_u^{\mathrm{H}} \boldsymbol{\Phi}_{u'} \boldsymbol{R} \boldsymbol{H}_{f,u'} + \boldsymbol{z}_u^{\mathrm{LS}}. \end{aligned} \tag{74}$$

Table 1 SCM simulation configurations

Channel model	Configurations
Scenario	Urban micro
Velocity	5 km/h
Carrier frequency	2 GHz
Cell radius	500 m

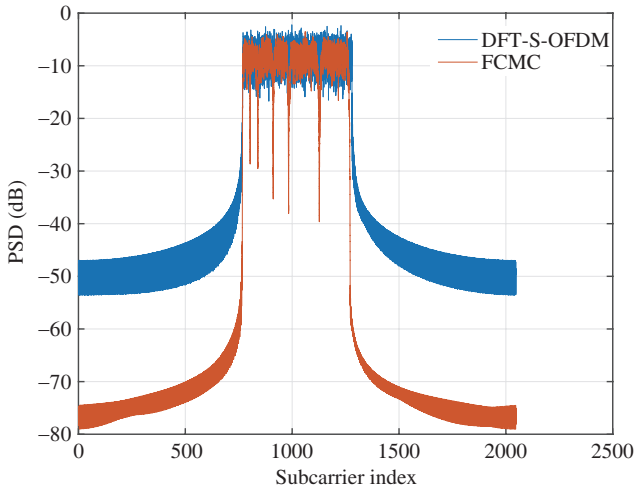

Figure 3 (Color online) FCMC and DFTS-OFDM PSD comparison.

When multiple UEs exist, subband filters are implemented in advance in order to eliminate interferences in different subchannels. The subband filters can be realized by fast convolution method in low complexity, and the frequency-domain filter is ideal bandpass filter. The filter implementation consists of three steps: (a) transforming the received overlapped pilot segment to frequency domain by M-points DFT; (b) multiplying the frequency domain pilot block by ideal bandpass filter coefficients; (c) transforming the pilot segment to the time domain by IDFT, and saving N out of M points. Therefore, the proposed pilot structure in (61) and the frequency domain CSI estimator in (71) can be extended to the FCMC-FDMA system with multiple UEs.

6 Simulation results

In this section, a simulation study is carried out to investigate the performance of the proposed FCMC receiver scheme based on FDMA. The channel matrices are generated by spatial channel model (SCM) with configurations set as Table 1. The main simulation system parameters are set as follows. The long transform length on the transmitter and receiver sides is fixed to $M = 2048$. The non-overlapping input block length is $N = 1024$. Each frame contains 14 data segments and a pilot segment.

Figure 3 compares power spectral density (PSD) of FCMC with discrete Fourier transform spread orthogonal frequency division multiplexing (DFT-S-OFDM). DFT-S-OFDM occupies 512 effective subcarriers with 2048-points FFT. In the FCMC system, different subband configurations are set, which illustrates the high flexibility and convenience to meet the diverse requirements of subbands. FCMC has a total of 6 subbands with 3 dB bandwidth 32, 32, 64, 64, 128, 128 FFT frequency intervals, respectively. RRC filters with rolloff factor 0.125 are used as filter banks. In such configurations, FCMC and DFT-S-OFDM can be compared with similar total bandwidth. Figure 3 shows that the FCMC system has lower sidelobe and OOBE compared with DFT-S-OFDM. The OOBE of FCMC is lower than -60 dB, and that of DFT-S-OFDM is about -40 dB.

Figure 4 shows the frequency domain window coefficients of RRC filter and the optimized filter. Figures 5 and 6 depict the normalized mean square error (NMSE) and the PSD performance comparison of

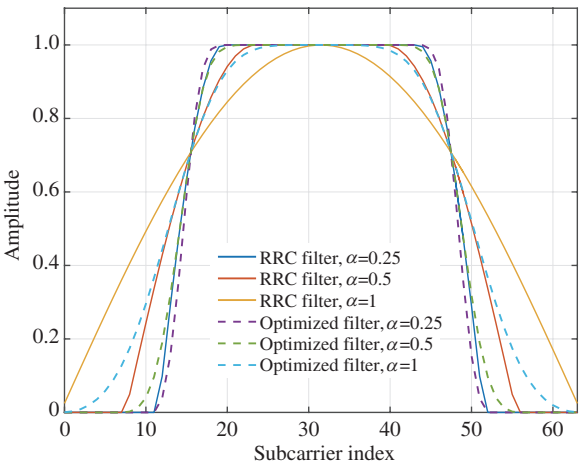

Figure 4 (Color online) Frequency domain window of RRC and the optimized filter.

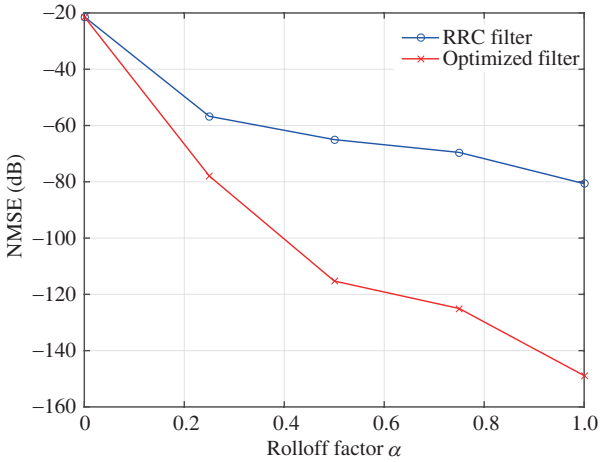

Figure 5 (Color online) NMSE performance comparison against the filter length.

the optimized filter and the RRC filter in FCMC system. In the simulation, we consider this scenario that oversampling factor is $N_r = 64$, thus the corresponding 3 dB bandwidth is $M_b = 32$. From Figure 5, it can be observed that the optimized filter NMSE significantly outperforms the conventional RRC filter over the whole range of occupied subcarriers. Moreover, as subcarriers number increasing, the number of subcarriers that can be optimized increases, thus the optimized filter has a larger NMSE performance gain compared to RRC filter. As shown in Figure 6, the interband interference of FCMC system utilizing optimized filter banks is about -60 dB, which is much lower than those applying RRC filters as synthesis and analysis filter banks.

Figure 7 shows the bit error rate (BER) performance of the proposed one-tap equalizers for $U = 1$ and $U = 5$. In this simulation, we consider the scenario that oversampling factor $N_r = 16$. RRC filter with rolloff factor $\alpha = 0.5$ is applied as filter banks. Binary data streams are encoded by Turbo code with rate 0.5. In this figure, 'ideal' and 'approximate' represent the proposed one-tap equalizer and low-complexity one-tap equalizer, respectively. Due to the interference reduction brought by filter banks, multiple users access makes little difference to BER performance. As expected, the proposed one-tap equalizers have similar BER performance on the whole SNR range both under the frequency selective channel and the flat fading channel. This implies that the one-tap channel equalizer can be properly simplified without performance degradation in the physical frequency selective channel. However, the BER under the frequency selective channel suffers a performance loss against that of the flat fading channel.

Figure 8 illustrates the effect of the pilot length on the channel estimation NMSE performance. The rolloff factor for RRC filter bank is $\alpha = 0.125$. In addition, the oversampling factor is $N_r = 16$. The Rayleigh fading channel is used. Assume that tap coefficients within the effective range of the filter are greater than 0.01 times the maximum tap coefficient. Under this circumstance, causal and non-causal part of effective CIR length is about 123 and 110. We can find that with the increase of the SNR, channel estimation NMSE with pilot length of 8 and 16 has the floor of -20 dB and -22 dB separately. As the oversampled length of CP and CS is smaller than CIR length, interferences induced by pilot is not sufficient to accurate CIR estimation. It is also shown that NMSE performance of channel estimation with pilot length of 32 and 64 is similar. We remark that to have reasonable channel estimation error with larger SNR, the circular prefix and suffix length should be larger than effective channel causal and non-causal part length separately. Figure 8 also compares the NMSE performance of the proposed channel estimation method with the classic method where CIR is estimated by calculating cross-correlation of the received pilot segment and the effective pilot. In this figure, 'proposed' and 'classic' represent the NMSE performance of the proposed channel estimation method and the classic method separately. As shown in Figure 8, the performance of these methods is nearly the same for all cases. However, the proposed

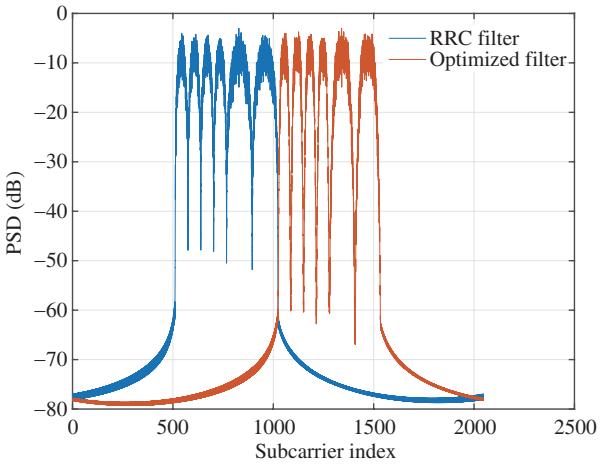

Figure 6 (Color online) Transmitted baseband signal PSD performance comparison against the filter length.

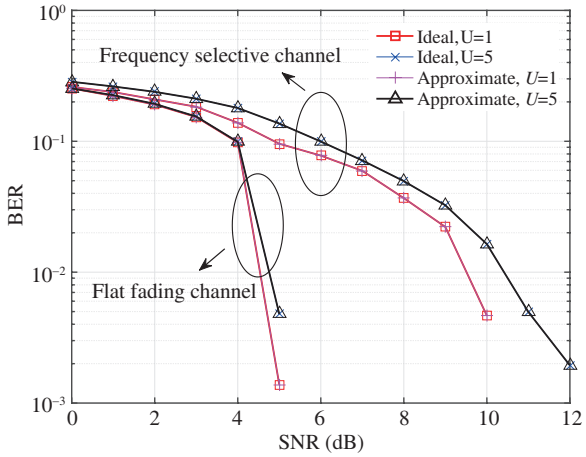

Figure 7 (Color online) BER performance comparison of the proposed equalizers under the frequency selective channel and the flat fading channel.

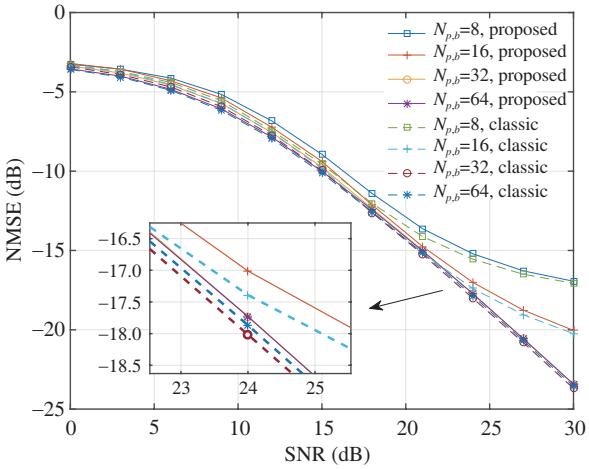

Figure 8 (Color online) NMSE performance comparison of the proposed and classic channel estimation method with different pilot length $N_{p,b}$.

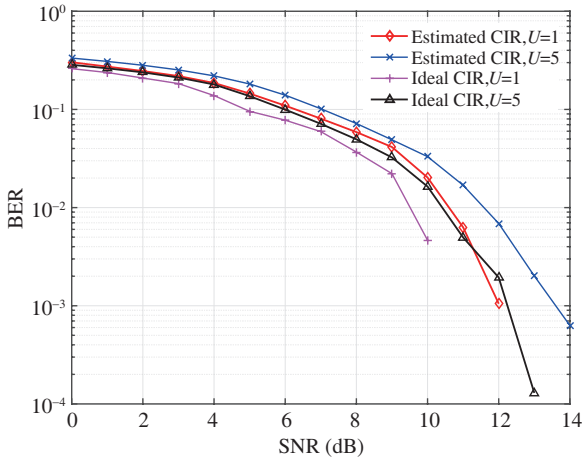

Figure 9 (Color online) BER performance comparison of considered equalizers under the SCM.

method has lower computation complexity by implementing channel estimation in the frequency domain.

Figure 9 compares the BER performance between FCMC system with known and unknown CIR in receiver. In this simulation, SCM is applied to generate multipath channel. FCMC transceiver configurations are the same as that of Figure 8. Although the FCMC system with known CIR outperforms that with unknow CIR, the BER performance gap between them is small. We can conclude that the estimator can obtain CIR efficiently with pilot assistance.

7 Conclusion

In this paper, we have investigated the filter bank optimization, as well as receiver design for FCMC based FDMA. By minimizing the IBI of transmitted signal under the filter energy and subcarriers range constraints, we have proposed the NPR filter banks optimization method. The MMSE criterion is then applied to calculate the coefficients of one-tap frequency domain equalizer. Moreover, to decrease equalizer computational complexity, the low-complexity one-tap equalizer has been further developed, which exploits the fact that Toeplitz matrices can be asymptotically diagonalized by DFT matrix. To obtain CSI required by channel equalization, we have proposed a combined CP and CS pilot structure and

corresponding frequency domain CSI estimation method. Simulation results confirm the powerfulness of the proposed channel estimator and equalizer based on FC structure.

Acknowledgements This work was supported in part by National Natural Science Foundation of China (Grant Nos. 61320106003, 61761136016, 61631018), Natural Science Foundation of Jiangsu Province (Grant No. BK20170688), National Science and Technology Major Project of China (Grant No. 2017ZX03001002-004), and Civil Aerospace Technologies Research Project (Grant No. D010109).

References

1 Ji X S, Huang K Z, Jin L, et al. Overview of 5G security technology. Sci China Inf Sci, 2018, 61: 081301
2 Li L M, Wang D M, Niu X K, et al. mmWave communications for 5G: implementation challenges and advances. Sci China Inf Sci, 2018, 61: 021301
3 Wunder G, Jung P, Kasparick M, et al. 5GNOW: non-orthogonal, asynchronous waveforms for future mobile applications. IEEE Commun Mag, 2014, 52: 97–105
4 Gupta A, Jha R K. A survey of 5G network: architecture and emerging technologies. IEEE Access, 2015, 3: 1206–1232
5 Ma Z, Zhang Z Q, Ding Z G, et al. Key techniques for 5G wireless communications: network architecture, physical layer, and MAC layer perspectives. Sci China Inf Sci, 2015, 58: 041301
6 Bellanger M, Le Ruyet D, Roviras D, et al. FBMC Physical Layer: a Primer. PHYDYAS FP7 Project Document. 2010
7 Jiang T, Chen D, Ni C X, et al. OQAM/FBMC for Future Wireless Communications: Principles, Technologies and Applications. Pittsburgh: Academic Press, 2017. 25–38
8 Kong D J, Xia X G, Jiang T. An Alamouti coded CP-FBMC-MIMO system with two transmit antennas. Sci China Inf Sci, 2015, 58: 102306
9 Michailow N, Matthe M, Gaspar I S, et al. Generalized frequency division multiplexing for 5th generation cellular networks. IEEE Trans Commun, 2014, 62: 3045–3061
10 Zhang X, Jia M, Chen L, et al. Filtered-OFDM - enabler for flexible waveform in the 5th generation cellular networks. In: Proceedings of 2015 IEEE Global Communications Conference, San Diego, 2015. 1–6
11 Vakilian V, Wild T, Schaich F, et al. Universal-filtered multi-carrier technique for wireless systems beyond LTE. In: Proceedings of 2013 IEEE Globecom Workshops, Atlanta, 2013. 223–228
12 Sahin A, Guvenc I, Arslan H. A survey on multicarrier communications: prototype filters, lattice structures, and implementation aspects. IEEE Commun Surv Tut, 2014, 16: 1312–1338
13 Boucheret M L, Mortensen I, Favaro H. Fast convolution filter banks for satellite payloads with on-board processing. IEEE J Sel Areas Commun, 1999, 17: 238–248
14 Borgerding M. Turning overlap-save into a multiband mixing, downsampling filter bank. IEEE Signal Process Mag, 2006, 23: 158–161
15 Renfors M, Harris F. Highly adjustable multirate digital filters based on fast convolution. In: Proceedings of 2011 20th European Conference on Circuit Theory and Design, Linkoping, 2011. 9–12
16 Renfors M, Yli-Kaakinen J, Harris F J. Analysis and design of efficient and flexible fast-convolution based multirate filter banks. IEEE Trans Signal Process, 2014, 62: 3768–3783
17 Shao K, Alhava J, Yli-Kaakinen J, et al. Fast-convolution implementation of filter bank multicarrier waveform processing. In: Proceedings of 2015 IEEE International Symposium on Circuits and Systems, Lisbon, 2015. 978–981
18 Renfors M, Yli-Kaakinen J, Levanen T, et al. Fast-convolution filtered OFDM waveforms with adjustable CP length. In: Proceedings of 2016 IEEE Global Conference on Signal and Information Processing, Washington, 2016. 635–639
19 Yli-Kaakinen J, Levanen T, Valkonen S, et al. Efficient fast-convolution-based waveform processing for 5G physical layer. IEEE J Sel Areas Commun, 2017, 35: 1309–1326
20 Yli-Kaakinen J, Renfors M. Flexible fast-convolution implementation of single-carrier waveform processing for 5G. In: Proceedings of 2015 IEEE International Conference on Communication Workshop, London, 2015. 1269–1274
21 Chen D, Qu D M, Jiang T. Novel prototype filter design for FBMC based cognitive radio systems through direct optimization of filter coefficients. In: Proceedings of 2010 International Conference on Wireless Communications and Signal Processing, Suzhou, 2010. 1–6
22 Chen D, Qu D M, Jiang T, et al. Prototype filter optimization to minimize stopband energy with NPR constraint for filter bank multicarrier modulation systems. IEEE Trans Signal Process, 2013, 61: 159–169
23 Tian Y, Chen D, Luo K, et al. Prototype filter design to minimize stopband energy with constraint on channel estimation performance for OQAM/FBMC systems. IEEE Trans Broadcast, 2018. doi: 10.1109/TBC.2018.2847453
24 Renfors M, Yli-Kaakinen J. Channel equalization in fast-convolution filter bank based receivers for professional mobile radio. In: Proceedings of the 20th European Wireless Conference, Barcelona, 2014. 1–5
25 Zhao J C, Wang W J, Gao X Q. Transceiver design for fast-convolution multicarrier systems in multipath fading channels. In: Proceedings of 2015 International Conference on Wireless Communications and Signal Processing, Nanjing, 2015. 1–5
26 Haykin S, van Veen B. Signals and Systems. New York: Wiley, 1999
27 Vaidyanathan P. Multirate Systems and Filter Banks. Upper Saddle River: Prentice-Hall, Inc., 1993
28 Yli-Kaakinen J, Renfors M. Optimized reconfigurable fast convolution-based transmultiplexers for flexible radio access. IEEE Trans Circ Syst II, 2018, 65: 130–134
29 Gray R. On the asymptotic eigenvalue distribution of Toeplitz matrices. IEEE Trans Inform Theor, 1972, 18: 725–730